

# On the Design of Coreless Permanent Magnet Machines for Electric Aircraft Propulsion

Damien Lawhorn, *Graduate Student Member, IEEE*, Peng Han\*, *Senior Member, IEEE*,  
Donovin Lewis, *Student Member, IEEE*, Yaser Chulaee, *Graduate Student Member, IEEE* and  
Dan M. Ionel, *Fellow, IEEE*

SPARK Lab, Department of Electrical and Computer Engineering, University of Kentucky, Lexington, KY, USA  
damien.lawhorn@uky.edu, donovin.lewis@uky.edu, yaser.chulaee@uky.edu, dan.ionel@uky.edu

\* ANSYS Inc., San Jose, CA, USA, peng.han@ieee.org

**Abstract**—This paper presents design and prototyping studies for coreless and slotless permanent magnet (PM) machines, which have the potential for high power density and efficiency, and discusses their feasibility for electric aircraft propulsion. The emphasis is on axial flux permanent magnet (AFPM) machines with printed circuit board (PCB) stators that have advantages over their wired counterparts in terms of design flexibility, coil accuracy, manufacturing process reliability, and heat dissipation. Detailed electromagnetic finite element analysis models were developed and employed alongside analytical sizing equations to evaluate the performance of two dual-rotor single-stator coreless AFPM designs employing wave and spiral PCB winding patterns. Design considerations for a 10kW 2,600rpm rating similar to the NASA X-57 electric aircraft propulsor motors are included. A 26-pole prototype machine has been developed and experimental testing results are presented.

## I. INTRODUCTION

Today, increased electrification of aircraft is becoming more feasible with recent advancements in electric propulsion components such as batteries, power electronics, and electric machines. Efficiency and power density play vital roles in determining if an electric machine is a viable option for aviation. Coreless and slotless machines offer benefits of high power/torque density, no cogging torque, low ripple, zero or negligible core losses, which contribute to a higher overall efficiency [1].

This paper presents example coreless axial flux permanent magnet (AFPM) machine designs and evaluates their suitability for electric propulsion. Considerations for the design and performance estimates of coreless AFPM machines for aircraft propulsion are discussed. Additionally, design, analysis, and prototyping of two variations of PCB stators have been conducted for 26-pole coreless AFPM machines.

The electrification of aircraft propulsion systems involve generating thrust, traditionally produced using combustion engines, with electric motors driving fans or propellers. To achieve this, machines with large power ratings, high reliability, low mass, and high efficiency are required. Alongside these requirements, low noise, vibration and harshness are desired traits. For practical implementations very high specific power is required with today's coreless and slotless electric motors achieving values in excess of 2.3kW/kg and, with NASA stating immediate future goals of 13kW/kg [2].

Attention has been drawn to coreless and slotless machines as potential aircraft motor topologies due to their potential high power density and efficiencies. Coreless and slotless machines are realized by the elimination of iron in the stator with non-magnetic supporting material or air. The absence of a magnetic core eliminates core losses, contributing to greater efficiencies, and results in zero cogging torque, which is favorable for low-noise and vibration applications. A survey of recent coreless and slotless machine designs and their associated performance indices is presented in Table I. These machines employ various stator winding implementations including multi-stranded wire, Litz wire and PCBs, including spiral, hexagonal, and wave windings. Specific powers of the machines ranges from 0.3 to 2.3 kW/kg. Among them, the coreless AFPM machines are more attractive due to their modularized nature and high integrity. Coreless and slotless machines can be designed to have a large variety of power ratings, ranging from tens to several mega watts.

For an estimate of the extended constant power speed range required, a design with a max speed 36% above the base speed was demonstrated in MagniX's cored AFPM motor used for short-haul electric aircraft [3]. Coreless machines typically have much smaller inductance than traditional cored electric machines, resulting in a lower maximum speed achievable using traditional field weakening techniques. Machines with a small inductance require a lower terminal voltage to operate at a given angular velocity, suggesting a higher base speed. Implementing techniques such as relative rotation of the stators discs as a means to reduce flux linkage or by using a controllable DC boost stage to the motor drive's input and use of a current weakening approach may allow constant power operation for the additional speed range required (Fig. 1).

## II. DESIGN CONSIDERATIONS AND PERFORMANCE ESTIMATES FOR CORELESS AFPM MACHINES

The direct exposure of stator windings to the air-gap in coreless AFPM machines implies that they are susceptible to significant ac losses in the conductors, particularly at high speed operation. As a result, wire wound stators using Litz wire, multiple smaller conductors, or PCB traces are often employed to combat the skin effect and reduce these losses

Stator Type	Rated Speed [krpm]	Power [kW]	Ref.
Slotless-RFPM	15	1,000	[4], [5]
Coreless-AFPM	15	250	[6]
Coreless-RFPM	6	37	[7]
Slotless-RFPM	6	32	[7]
PCB-AFPM (Dist.)	25	16	[8]
PCB-AFPM (Spiral)	1.8	11.2	[9]
Coreless-AFPM	1	2.25	[10]
Coreless-AFPM	0.4	0.67	[11]
Slotless-AFPM	10	0.5	[12]
PCB-AFPM (Hex.)	0.375	0.4	[13]
PCB-AFPM (Spiral)	7.5	0.28	[14]
PCB-AFPM (Wave)	3	0.18	[15]
PCB-AFPM (Hex.)	2	0.04	[16]

Table I  
EXAMPLE CORELESS AND SLOTLESS AXIAL AND RADIAL FLUX PERMANENT MAGNET (RFPM) ELECTRIC MACHINES BASED ON LITERATURE REVIEW.

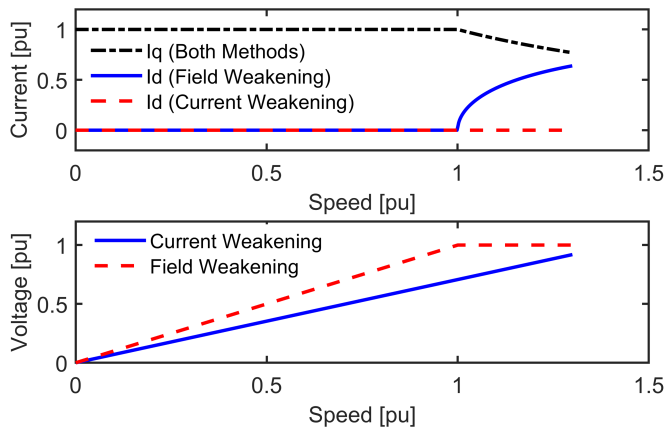


Fig. 1. Motor current and terminal voltage in field weakening and current weakening control for extended-speed constant-power operation. In electric aircraft propulsion applications, a range of only approximately 30% is required.

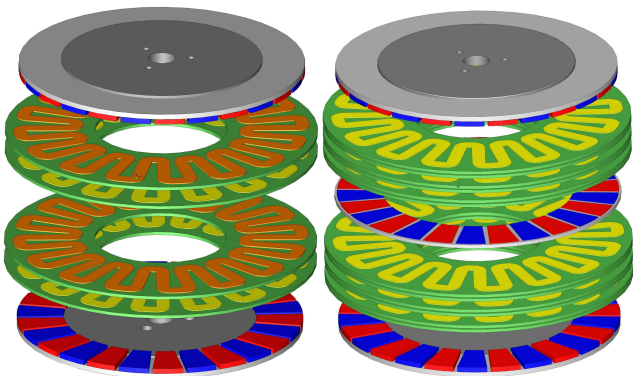


Fig. 2. For coreless machines, multiple stacks of stators and rotors can be employed in a modular approach to achieve a specified power rating.

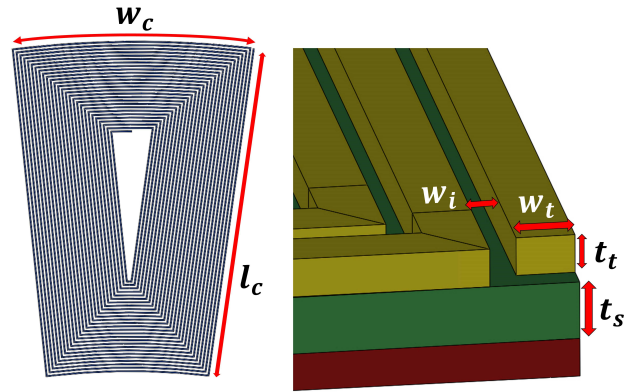


Fig. 3. Main geometric variables for PCB stators in coreless machines. The coil shown has a spiral pattern and connects to internal layers using vias.

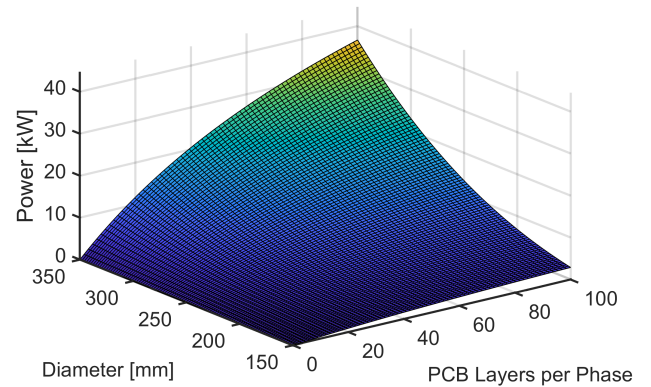


Fig. 4. Analytically estimated electromagnetic power output of a three-phase wave winding AFPM machine as the outer diameter and number of parallel layers per phase are varied. The results were calculated based on the PCB parameters and a constant value for the ration of outer to inner diameter, as presented in Table. II.

[17]. In addition to the ac losses, dc losses must be considered and are proportional to the winding resistance.

An AFPM machine's disk-shaped stator provides opportunities to implement the windings in unique ways, such as using PCBs. The fabrication process of PCBs is reliable, highly repeatable and has been proven in consumer electronics. Electric machine designers may make modifications to a stator's coil shape, track width, or winding configuration in professional circuit design software, with minimal impact to the manufacturing setup. PCB stators may also offer a modular approach to machine design specification as multiple boards may be stacked in parallel or series to increase speed or torque rating (Fig. 2). Design of the windings is a key factor in their overall effectiveness, defining a significant portion of the losses and related efficiency [18]. Geometric parameters for PCB stators include trace width, thickness, isolation distance, and substrate thickness, as shown in Fig.3.

Considering the modeling complexity and computation time, analytical equations are recommended within the design stage for initial sizing and torque estimation. The power output

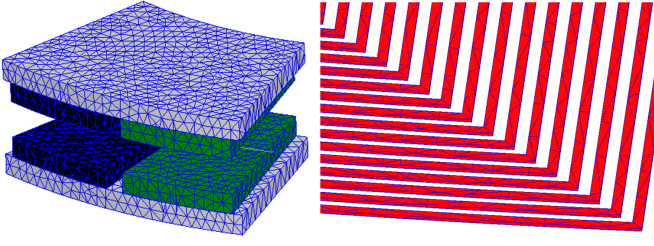


Fig. 5. Meshing of detailed trace-by-trace model of the proposed PCB spiral winding coreless AFPM machine. The rotor back iron and magnets are shown on the left and the PCB traces are shown on the right.

of a coreless AFPM machine is related to its rotor speed, dimensions, airgap flux density and the current loading, as expressed by:

$$P = \frac{B_m A \pi^2 n D_o^3 (1 - \lambda)(1 - \lambda^2)}{240\sqrt{2}}; \quad (1)$$

$$A = \frac{2NmI}{\pi D_m}; \quad \lambda = \frac{D_i}{D_o},$$

where  $P$  is the output power,  $B_m$  the peak flux density in the airgap,  $n$  the rotational speed, and  $D_o$  the outer diameter. When calculating the current loading,  $A$ ,  $m$  is the number of phases,  $D_m$  the mean diameter,  $D_i$  the inner diameter and  $N$  the number of turns in series per phase. The stator current,  $I$ , may be derived as:

$$I = Ja; \quad a = t_t w_t n_p, \quad (2)$$

where  $J$ , is the current density,  $a$  is the cross-sectional area of the copper in a coil, which in PCB stators, is a function of trace width,  $w_t$ ; thickness  $t_t$ ; and number of traces in parallel,  $n_p$ . While wire wound stators using Litz wire or multiple stranded wires may have a higher slot fill factor, PCB stators may allow a higher current density to compensate for the reduced copper area. Using these initial sizing equations and the assumptions that the ratio of outer to inner diameter remains constant and the PCB characteristics match those seen in the wave winding machine in Table I, power output was estimated as a function of outer diameter and number of PCB layers connected in parallel (Fig. 4).

For example, with the prototype machine diameter later described in this paper, to achieve an output power of 10.5kW as specified in the X-57 Maxwell electric aircraft, approximately 55 PCB layers in parallel are required. Typical state-of-the-art implementation for PCBs employs 12 layers per board. Magnets may need to be increased in size in order to compensate for the additional flux fringing and leakage.

Electromagnetic finite element analysis models, such as those discussed in [19], were built and used for performance and eddy current loss estimation of the 26 pole dual rotor PCB winding machine designs discussed later in this paper. The flux density of the rotor under a loaded condition with a wave winding stator is illustrated in Fig. 6. A trace-by-

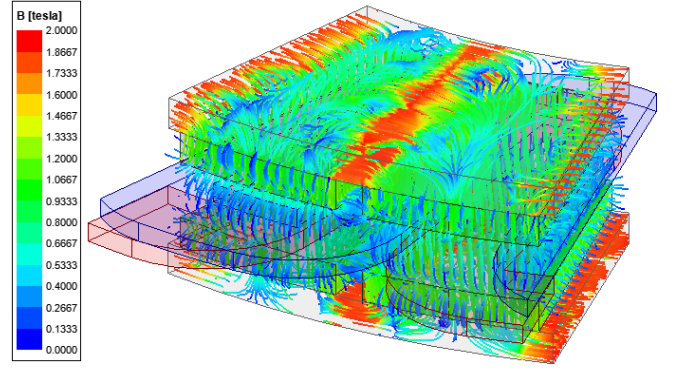


Fig. 6. Three dimensional view of the magnetic flux density of the prototype 26-pole dual-rotor motor design with a two-phase wave winding stator under loaded conditions.

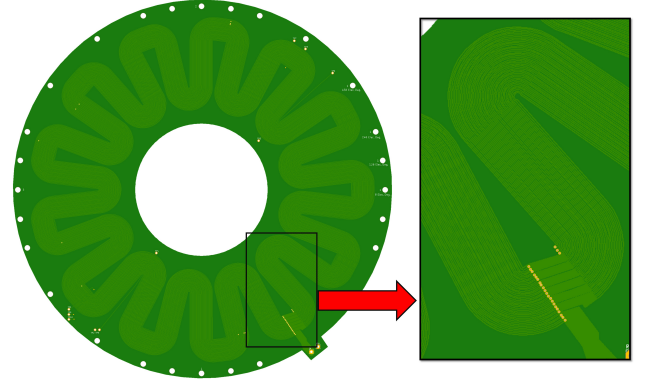


Fig. 7. Electronic computer-aided design (ECAD) rendering of the proposed wave winding PCB stator. Seven groups of six parallel traces are connected in series.

trace 3D representation was used in the winding analysis, leading to a very dense model with *26.4 million tetrahedral meshing elements*, as seen in Fig. 5. Such large models are computationally intensive, requiring over 72 hours to simulate a single electrical cycle on a high performance computing (HPC) cluster with 64 cores and 192 GB of RAM using Intel 6130 2.1GHz processors.

### III. WAVE WINDING

A wave winding PCB stator with 6 layers per board was designed and produced with 5 layers hosting active copper while the remaining layer is used as a path to route the return terminal to the outer diameter of the stator. On each of the active layers, there are 42 traces with a trace width,  $w_t$ , of 0.20mm and an isolation width,  $w_i$ , of 0.25mil. For the same layer, conductors are grouped in parallel connections of 6 traces, which are then connected in series to form 7 turns. The same wave pattern is repeated throughout 5 layers, all connected in parallel using vias as shown in Fig. 7.

The wire groups perpendicular to the magnetic field produced by the rotor magnets consist of independent traces, which vary in their distance from the magnets, both axially

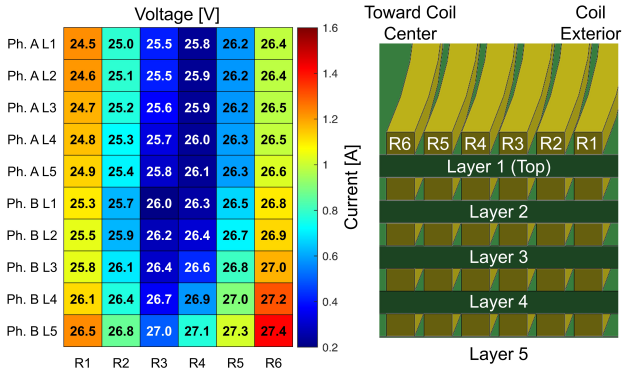


Fig. 8. Induced voltage values calculated by FEA and colormap for circulating currents in the traces composing one turn of the proposed wave winding PCB derived from FEA models.

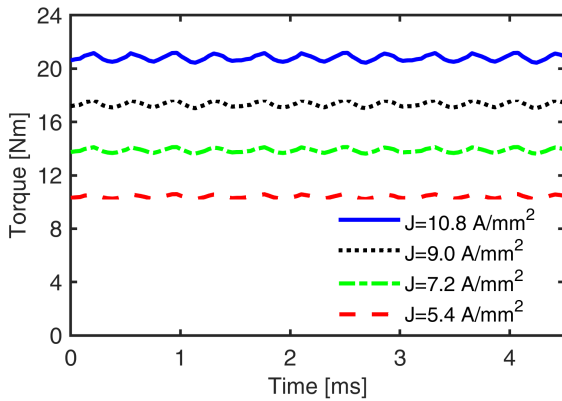


Fig. 9. FEA calculated torque of the proposed two-phase wave winding PCB coreless machine. Note the absence of saturation and the linear response of torque with current. The X-57 Maxwell uses 10.5kW high-lift motors at approximately 2,600rpm, therefore one alternative implementation is with two stator and three rotor modules.

and radially. This difference in observed magnetic field variations results in unequal induced voltage in each trace, which produces circulating currents. The in depth trace-by-trace FEA models allow detailed analysis of this effect and estimation of the machine's torque production. The induced voltage was used with the calculated trace resistance to estimate the resultant circulating currents as shown for the wave winding PCB in Fig. 8. The FEA models were also used to estimate the torque production of the machine (Fig. 9).

In electric aircraft applications such as the high-lift motors of NASA's X-57 Maxwell, a power rating of 10.5kW is required at a speed of 2,600rpm [20]. Assuming adequate cooling, such that a current density of  $10.8 \text{ A/mm}^2$  is acceptable, the FEA calculations show that the proposed machine design may produce approximately 21Nm of torque. Based on these results, an alternative implementation for these electric aircraft motors may be achieved by means of a coreless AFPM machine with two stator and three rotor axially modules.

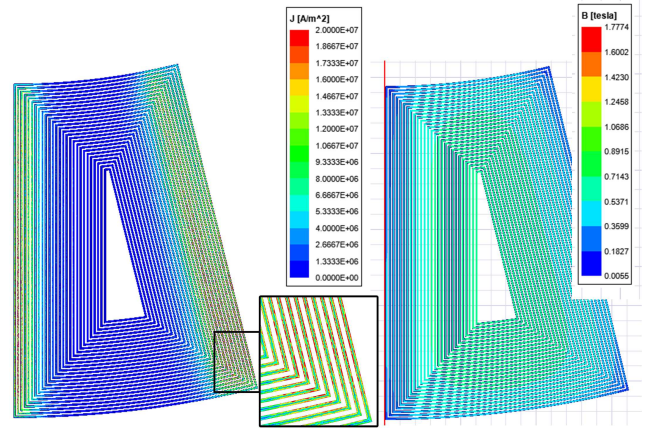


Fig. 10. FEA results of current density distribution and flux density distribution in a spiral type PCB stator coil under open-circuit condition at 3,050r/min. Current is most highly concentrated at the edges of traces due to the eddy effect.

#### IV. SPIRAL WINDING

The designed spiral winding PCB stator utilizes 6-layers per board, as seen in the previous wave winding design. Assuming an even number of layers is used, this winding technique allows both the input and return terminals to end on the outer diameter of the PCB. This eliminates the need for a return path layer and allow all layers to host active copper. The coil shape used in the design and development of this prototype has a coil width,  $w_c$ , of 20mm and a coil length,  $l_c$ , of 30mm. Each coil contains 27 loops of traces with 0.20mm and 0.25mm for  $w_t$  and  $w_i$  respectively. For this prototype, the  $t_t$  is 0.139mm, which corresponds to  $4oz/ft^2$ .

A trace located on the coil inner side completes the connection at the input terminal on the top layer of the board to create 27 parallel loops. At this position, a via transitions the connection from an odd numbered layer to an even layer. The same coil winding direction was then continued until the trace reaches active portion of the stator's outer diameter at the end of the loop with a via being used to repeat the pattern to the next layer. By constraining the total layer count to an even number, the traces may easily be brought out to the return terminal without a dedicated return path layer, necessary in the wave winding PCB. This maximizes the layers with active copper, and subsequently, increases the equivalent fill factor of the stator. Input and return bus bars were included along the circumference to connect the windings and ensure opposite polarity between adjacent coils. Based on the described spiral winding machine design, FEA models were created and used to simulate operation under open-circuit conditions. Example results include the current density and flux density, as demonstrated in Fig. 10.

#### V. DEMONSTRATOR OF A CORELESS AFPM MACHINE WITH PCB STATORS

Design, simulation, and prototyping has been conducted for variations of PCB stator topologies for 26-pole coreless AFPM

Table II  
MAIN DESIGN DATA FOR PROTOTYPE PCB CORELESS AFPM MACHINES.

Rotor	
Rotor OD [mm]	270.4
Rotor ID [mm]	182
Pole pitch at ID [mm]	17.2
Pole pitch at OD [mm]	28.8
Magnet thickness [mm]	5
Back iron thickness [mm]	10
Wave Winding PCB Stator	
Stator ID [mm]	144.5
Stator OD [mm]	304.9
Active layers	5
Trace width/isolation, $w_t/w_i$ [mm]	0.20/0.25
Trace thickness, $t_t$ [mm]	0.07
Trace length [m]	8
Spiral Winding PCB Stator	
Stator ID [mm]	1182
Stator OD [mm]	270.4
Active layers	6
Trace width/isolation, $w_t/w_i$ [mm]	0.20/0.25
Trace thickness, $t_t$ [mm]	0.14
Trace length [m]	14

machines with dual rotors. A first prototype utilizes a wave-type winding as shown in Fig. 7. A single PCB uses 6-layers, 5 of which in series using vias located at the interior and exterior of the coil to connect adjacent layers.

A second prototype employs a spiral-type winding with the same trace width, isolation and layer count as the first prototype. Both of the mentioned stators use the same 26-pole dual rotor and the main dimensions of the components are shown in Table II.

The prototype PCB stators were designed in ECAD software and produced as a modular set of boards to be connected in parallel. The machine was assembled with an angular displacement of each phase module for the appropriate electric degrees offset. Mounting holes were included on the outer diameter of the PCB stators to allow angular displacement for 120 elec. degrees offsets, used in a three-phase machine, or 90 electrical degrees offset for a two phase configuration.

To evaluate the prototype wave winding machine's performance, a mechanical testing fixture has been constructed to accommodate various stator configurations and alternate PCB stators, as shown in Fig. 11. Axial-flux machines are particularly difficult to assemble considering the substantial axial magnetic force, in this case, between the dual rotors. A rotor attachment and removal tool was specially manufactured to allow precise, controlled axial displacement of the second rotor. With the first rotor fixed in place, the tool attaches to the second rotor and was used to lower it into position.

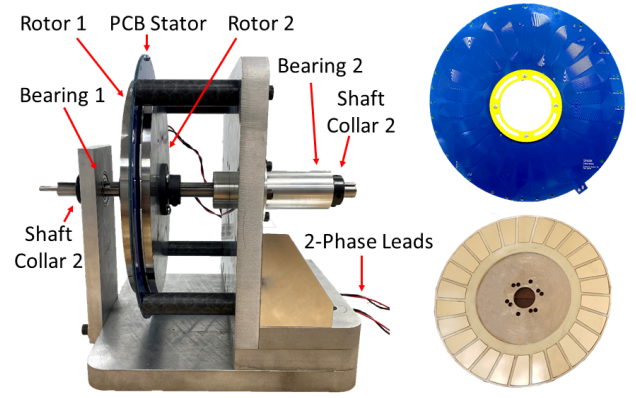


Fig. 11. Prototype dual rotor AFPM machine and special testing fixture. The machine employs a wave winding PCB stator in the schematic diagram. The PM rotor (top right) and the prototype PCB stator (bottom right) are shown disassembled.

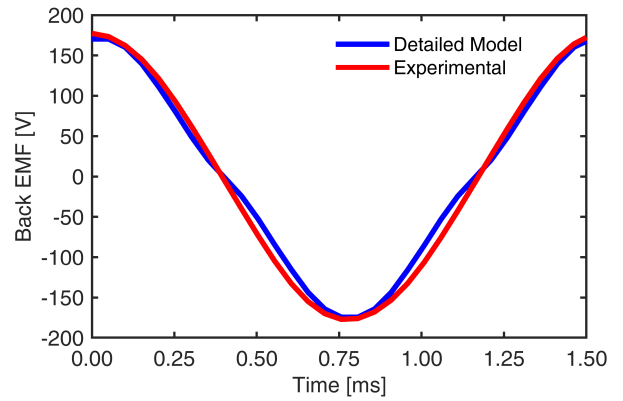


Fig. 12. Simulated and experimental open-circuit back emf at 3050rpm. The wave winding machine tested utilizes (4) PCBs, comprising 2-phases.

The conditions of the experiment and simulation were set the same for validation studies with two phases and a spacing of 7mm between the rotors. A prime mover was then attached to the machine's shaft and used to rotate the machine up to a speed of 3,050rpm. The open-circuit induced back emf was recorded and compared to the simulated results (Fig. 12).

The test setup previously described was then used to operate the machine as an uncontrolled generator connected to a resistive load of 6.5  $\Omega$  per phase. The prime mover was used to drive the generator at speeds that produced significant current in the windings. For example, 5A of current corresponds to a current density in the stator windings of approximately 6A/mm<sup>2</sup>. The output currents of the machine were measured and are shown in Fig. 13. For this test, a thermal imaging camera captured the temperature at the PCB windings (Fig. 14).

## VI. CONCLUSION

This paper has explored the feasibility of coreless machines, especially with an axial flux topology with PCB stators, as potential candidates for electric aircraft propulsion applications.

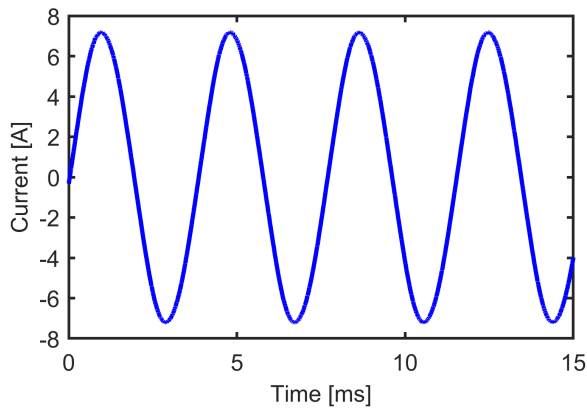


Fig. 13. Output current of the prototype machine operating as an uncontrolled generator feeding a purely resistive load of 6.5 Ohms.

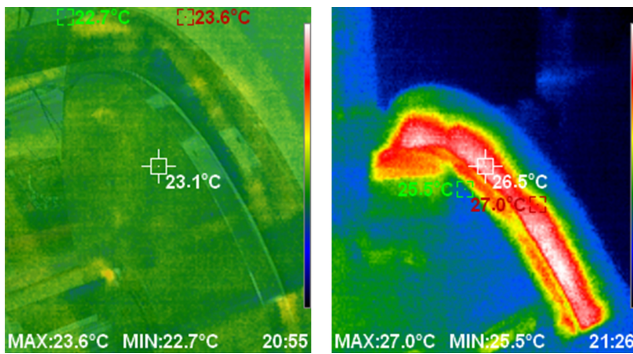


Fig. 14. Temperature distribution on the prototype wave winding PCB stator under a generator loaded condition detailed in Fig. 13. Measurements were taken prior to test, as seen on the left, and after the machine was operated at a current density of  $6 \text{ A/mm}^2$  for 5 minutes, shown on the right.

The study included a literature review of recently reported related developments, an initial sizing based on closed form analytical equations, followed by extensive electromagnetic 3D FEA on very large problems with tens of millions of tetrahedral meshing elements. A prototype using two 26-pole rotors and a single PCB stator has been designed, built, and tested. Based on combined simulation and experimental results, it is estimated that for a PCB current density suitable for high performance cooling, a rating typical for the propulsion motors of multi-propeller small aircraft, i.e. 10kW at 2,600rpm, can be achieved using multiple PCBs with parallel layers or an axially modular alternate arrangement with 3 rotors and 2 stators.

#### ACKNOWLEDGMENT

The support of the National Aeronautics and Space Administration (NASA) for research on electric aircraft power systems and components through the NASA Grant no. KY GF-20-055 and of the National Science Foundation (NSF) for research on special electric machines and power electronics drives through the NSF Award # 1809876 is gratefully acknowledged. Any opinions, findings, and conclusions or recommendations expressed in this material are those of the authors and do not necessarily reflect the views of the NASA or the NSF. The support of University of Kentucky, the L. Stanley

Pigman Endowment, of ANSYS, Inc., and of Regal Beloit Corp. is also gratefully acknowledged.

#### REFERENCES

- [1] N. Taran, V. Rallabandi, and D. M. Ionel, "WAVED: A coreless axial flux PM motor for drive systems with constant power operation," in *2019 IEEE Transportation Electrification Conference and Expo (ITEC)*, 2019, pp. 1–6.
- [2] R. Del Rasario, "A future with hybrid electric propulsion systems: A NASA perspective," *Turbine Engine Technology Symposium*, 2014.
- [3] "Magnix," accessed 08 Jan, 2020. [Online]. Available: <https://www.magnix.aero/products>
- [4] A. Yoon, X. Yi, J. Martin, Y. Chen, and K. Haran, "A high-speed, high-frequency, air-core PM machine for aircraft application," in *2016 IEEE Power and Energy Conference at Illinois (PECI)*, 2016, pp. 1–4.
- [5] A. D. Anderson, Y. Wang, Y. Yu, and K. S. Haran, "Experimental validation of a high-power slotless stator," in *2019 IEEE International Electric Machines Drives Conference (IEMDC)*, 2019, pp. 1564–1569.
- [6] Z. Zhang, W. Geng, Y. Liu, and C. Wang, "Feasibility of a new ironless-stator axial flux permanent magnet machine for aircraft electric propulsion application," *CES Transactions on Electrical Machines and Systems*, vol. 3, no. 1, pp. 30–38, 2019.
- [7] Z. Song, C. Liu, and H. Zhao, "Comparative analysis of slotless and coreless permanent magnet synchronous machines for electric aircraft propulsion," in *2019 22nd International Conference on Electrical Machines and Systems (ICEMS)*, 2019, pp. 1–6.
- [8] D. D. Tremelling, "On the design and analysis of a printed circuit board in a high speed surface permanent magnet axial flux machine," Ph.D. dissertation, University of Wisconsin-Madison, 2009.
- [9] P. Guedes-Pinto, "High efficiency axial flux PM machines," Aug 2020.
- [10] F. Profumo, A. Tenconi, M. Cerchio, J. F. Eastham, and P. C. Coles, "Axial flux plastic multi-disc brushless pm motors: performance assessment," in *Nineteenth Annual IEEE Applied Power Electronics Conference and Exposition, 2004. APEC '04.*, vol. 2, 2004, pp. 1117–1123 vol.2.
- [11] M. Aydin, M. Gulec, Y. Demir, B. Akyuz, and E. Yolacan, "Design and validation of a 24-pole coreless axial flux permanent magnet motor for a solar powered vehicle," in *2016 XXII International Conference on Electrical Machines (ICEM)*, 2016, pp. 1493–1498.
- [12] M. S. Islam, R. Mikail, and I. Husain, "Slotless lightweight motor for aerial applications," *IEEE Transactions on Industry Applications*, vol. 55, no. 6, pp. 5789–5799, 2019.
- [13] X. Wang, C. Li, and F. Lou, "Geometry optimize of printed circuit board stator winding in coreless axial field permanent magnet motor," in *2016 IEEE Vehicle Power and Propulsion Conference (VPPC)*, 2016, pp. 1–6.
- [14] X. Wang, C. Hu, M. Zhao, L. Wu, and S. Zhou, "Design of multi-layer pcb coreless axial permanent magnet synchronous motor," in *2019 22nd International Conference on Electrical Machines and Systems (ICEMS)*, 2019, pp. 1–4.
- [15] F. Marignetti, G. Volpe, S. M. Mirimani, and C. Cecati, "Electromagnetic design and modeling of a two-phase axial-flux printed circuit board motor," *IEEE Transactions on Industrial Electronics*, vol. 65, no. 1, pp. 67–76, 2018.
- [16] F. Tokgöz, G. Çakal, and O. Keysan, "Design and implementation of an optimized printed circuit board axial-flux permanent magnet machine," in *2020 International Conference on Electrical Machines (ICEM)*, vol. 1, 2020, pp. 111–116.
- [17] M. G. Kesgin, P. Han, N. Taran, D. Lawhorn, D. Lewis, and D. M. Ionel, "Design optimization of coreless axial-flux PM machines with Litz wire and PCB stator windings," in *2020 IEEE Energy Conversion Congress and Exposition (ECCE)*, 2020, pp. 22–26.
- [18] X. Wang, C. Li, and F. Lou, "Geometry optimize of printed circuit board stator winding in coreless axial field permanent magnet motor," in *2016 IEEE Vehicle Power and Propulsion Conference (VPPC)*, 2016, pp. 1–6.
- [19] M. Rosu, P. Zhou, D. Lin, D. M. Ionel, M. Popescu, F. Blaabjerg, V. Rallabandi, and D. Staton, *Multiphysics Simulation by Design for Electrical Machines, Power Electronics and Drives*. Wiley, 2018.
- [20] Y. Gibbs, "NASA Armstrong Fact Sheet: NASA X-57 Maxwell," Sep 2018, accessed: May, 2021. [Online]. Available: <https://www.nasa.gov/centers/armstrong/news/FactSheets/FS-109.html>